THEORETICAL AND EXPERIMENTAL INVESTIGATIONS OF THE PHYSICS OF CRYSTALLINE SURFACES

Principal Investigator: E. Bauer

Second Quarterly Status Report
For the Period 1 May-31 July 1966

Prepared for the
National Aeronautics and Space Administration
Washington, D. C.

GPO PRICE $ _____

Fund Transfer R-05-030-00 CFSTI PRICE(S) $ _____

Hard copy (HC) 3.00

Microfiche (MF) .75

ff 653 July 65

U. S. Naval Ordnance Test Station
China Lake, California

Second Quarterly Status Report
Fund Transfer No. R-05-030-001
For the Period 1 May-31 July 1966

I. The relation between structure of epitaxial films and surface and interfacial energies (A. K. Green and E. Bauer).

The interpretation and discussion of the epitaxy of f.c.c. metals on alkali halides with different surface conditions in ultrahigh vacuum has been completed (Encl. (1)). Preparations are being made for quantitative studies involving radiotracer measurements in addition to the presently used techniques. Studies of the growth of alkali halides on alkali halides have been resumed (now on surfaces cleaved in ultrahigh vacuum) in order to obtain an understanding of the observations made in ordinary vacuum (A. K. Green, E. Bauer, J. Appl. Phys. 37, 917 (1966).

II. Quantitative studies of the elastic and inelastic interactions of slow electrons with W single crystal surfaces (J. O. Porteus).

Preliminary measurements of the intensity of the (00) beam from a tungsten (110) surface have been made as the angle of incidence was varied. A lack of reproducibility was noted and was tentatively attributed to recontamination of the surface after cleaning. Analysis of desorbed gas with a mass spectrometer indicated considerable CO contamination of the sample during the scanning interval. Also, desorption rates are indicative of inadequate pumping speed. Plans are under way to convert from oil-diffusion to ion pumping in an effort to produce an adequate vacuum environment for these experiments.

III. Determination of nature and structure of surface layers with low energy electron diffraction (E. Bauer).

All work was concerned with the structure of SrO layers on the W (110) plane (see IV).

IV. Relation between structure and electron emission properties of work function reducing layers on W{110} planes (G. Turner and E. Bauer).

The work with SrO layers (see first quarterly status report) has been continued, revealing a very complex dependence of the emission properties on film thickness, deposition or annealing temperature and annealing time. This complex dependence had led to an incorrect tentative association between structure and emission properties (see first quarterly status report) which is corrected in the oral presentation of the paper (Encl. (2)). More work will be needed to obtain a fully reliable association between surface structure and emission properties of this system.

V. Momentum exchange of atoms on well defined single crystal surfaces (W. Faith and E. Bauer).

The molecular beam attachment for the low energy electron diffraction system has been nearly completed and will be tested in situ during the next quarter, in which also the first measurements are expected.

VI. Theory of low energy electron scattering (E. Bauer).

Our claim that relativistic effects are important in the scattering of slow electrons by neutral atoms (H. N. Browne, Phys. Rev. Letters 16, 495 (1966) has caused considerable controversy, which is clarified in Encl. (3).

PUBLICATIONS

1. "On the Formation of Single Crystal Films of f.c.c. Metals on Alkali Halide Cleavage Planes. II. Comparison of Experiment and Theory," by E. Bauer and A. K. Green, submitted to phys. stat. solidi.

2. "An Ultrahigh Vacuum Electron Microscope and its Application to Work Function Studies," by G. H. Turner and E. Bauer, to be presented at the International Congress on Electron Microscopy in Kyoto, Japan, August/September 1966.

3. "Importance of Relativistic Effects in the Scattering of Slow Electrons by Atoms II," by H. N. Browne and E. Bauer, submitted to Phys. Rev. Letters.

On the Formation of Single Crystal Films of f.c.c. Metals on Alkali Halide Cleavage Planes

II. Comparison of Experiment and Theory

E. Bauer and A. K. Green
Michelson Laboratory, China Lake, California 93555

ABSTRACT

The experimental results of Part I are compared with theory and with other relevant experimental work. Emphasis is placed on the influence of the substrate surface condition and of residual gases on the film growth. The film growth is subdivided into three stages: (1) the nucleation and initial growth stage, (2) the coalescence stage, and (3) the filling-in stage. The discussion of stage (1) shows that phenomenological nucleation theory can best account for the observations and that the epitaxial orientation develops most probably during the initial growth of the crystals. In stages (2) and (3) the interfacial energy between the crystals and their free surface energy play a major role in determining the coalescence process. The importance of the twin boundary energy and of chemical reactions is emphasized. The discussion shows that the growth of f.c.c. metals on alkali halides is highly specific for each film-substrate pair and the experimental conditions and that the lattice mismatch is an unimportant parameter.

Encl. (1)

Die experimentellen Ergebnisse des ersten Teils (I) werden mit der Theorie und anderen einschlägigen Experimenten verglichen. Das Schwergewicht liegt auf dem Einfluss des Oberflächenzustandes und von Restgasen auf das Filmwachstum. Das Filmwachstum wird in 3 Phasen aufgeteilt: (1) Keimbildung und Anfangswachstum, (2) Koaleszenz und (3) Auffüllphase. Die Diskussion der Phase (1) zeigt dass die phänomenologische Keimbildungstheorie am besten die Beobachtungen erklären kann und dass die epitaxiale Orientierung sich höchstwahrscheinlich im Anfangswachstum ausbildet. In den Phasen (2) und (3) spielt die Grenzflächenenergie zwischen den Schichtkristallen und ihre Oberflächenenergie die wichtigste Rolle für die Koaleszenz. Die Wichtigkeit der Zwillingsgrenzenenergie und von chemischen Reaktionen wird hervorgehoben. Die Diskussion zeigt, dass das Wachstum von k.f.z. Metallen auf Alkalihalogeniden äusserst spezifisch für jeden Film-Unterlagenparr und für die experimentellen Bedingungen ist und dass dabei der Gitterkonstantenunterschied nur eine unwesentliche Rolle spielt.

1. Definition of Growth Stages

We divide the process of formation of single crystal films into three stages: (1) the nucleation and initial growth stage, (2) the coalescence stage, and (3) the filling-in stage. These stages are characterized in the following manner. In stage (1), nuclei form continuously and grow but are sufficiently far apart that they do not contact each other to a significant amount. However their diffusion regions--i.e. the regions which supply the growing crystals with atoms--may overlap. Stage (2) is dominated by the formation of larger crystals from smaller crystals by

coalescence or simply growing together. Although the coalescing smaller crystals may have formed at different times and grown at different rates, they have nevertheless comparable size. This is not true in stage (3) in which there are large differences in size between the crystals formed by coalescence in stage (2) and those which have not coalesced or have nucleated in stage (2) or (3). Stage (3) includes Pashley's network, channel and hole stages.

2. Nucleation and Initial Growth Stage

2.1. Surface condition

It is obvious that the condition of the surface has a profound influence on the film formation. It determines the thermal accommodation of the hot vapor beam, the heat of adsorption, the activation energy for surface diffusion, the absolute value and orientation dependence of the binding energy of the cluster to the substrate and the interfacial energy between film crystal and substrate. There is little doubt now that an alkali halide surface not cleaved in UHV is covered with a surface layer. The nature and thickness of this layer depends upon the environment, temperature and duration of exposure of the cleavage plane. Of the several views of the structure of air cleaved alkali halide surfaces presently being held [5,25-27], we accept the hydrated surface layer model [25-27] here, but do not exclude the possibility that CO or CO_2 is also present in this layer. Our RED comparison of the UHV and air cleaved surfaces after a bakeout for several hours below 250°C shows that the lateral periodicity of this surface layer is the same as that of clean NaCl or KCl, but the increased background indicates that the degree of order in the layer is

lower than on the vacuum cleaved surface. This is in agreement with LEED observations. The positions of the H_2O, CO or CO_2 molecules and the thickness of the layer together with their temperature and time dependence (pre-annealing!) is difficult to determine at present. The growth of Au films indicates that the layer is removed after 48 hours annealing at 360°C or 1 hour annealing at 450°C in UHV. Harsdorff's water multilayer model is discounted for two reasons: (1) the mass spectrometer evidence [28] is not tenable [12,28], and (2) the predictions of the model are not in agreement with our observations discussed in 2.2. and 2.3.

2.2. Number and size of crystals

The results reported in Part I and elsewhere [12] clearly indicate that the number of crystals on UHV cleaved surfaces is much smaller than on air cleaved surfaces. This agrees qualitatively with Jaunet and Sella's [7] and Matthews' [14] results, but there are considerable quantitative differences as can be seen by comparing Table 1 of Part I with Table 1, which gives data from some other evaporations of f.c.c. metals onto crystals with NaCl structure. These differences are however not surprising: In Jaunet and Sella's [7] work, cleaving and deposition took place in ordinary vacuum and at room temperature, the film crystals were at least partially coalesced; Matthews [14] deposited his films at 360°C. In our own results at 360°C the ratio of the particle numbers N_{air}/N_{UHV} varies from ∞ (i.e. no particles on the UHV cleaved side, $\sim 10^{10}$ on the air cleaved side) to $\gtrsim 1$, depending upon deposition conditions. However our absolute particle numbers at 360°C are always much smaller than Matthews' which may be due to differences in gas composition (baked versus unbaked system!), rate, thickness, and other parameters. The rate and thickness dependence is illustrated by

the increase in particle number from $2.5 \cdot 10^{10}$, in the thinnest part usable for particle counting of a wedge film on a vacuum cleaved KCl surface, to a maximum of $15 \cdot 10^{10}$ before large scale coalescence reduces the particle number.

In spite of the strong dependence of the absolute and relative particle number on many parameters the following general qualitative rules apply for the difference between air cleaved and vacuum or UHV cleaved surfaces, at least for the materials investigated so far: (1) the formation of crystals begins on the UHV cleaved surface later than on the air cleaved surface; (2) the initially observed crystals are larger on the UHV cleaved surface than on the air cleaved surface; (3) the number N_{UHV} (or N_{vac}) of crystals on the UHV (or vacuum) cleaved surface is much smaller than the number N_{air} of crystals on the air cleaved surface; (4) the difference between N_{UHV} and N_{air} for a given crystal is much larger than the difference between the N_{UHV}'s or N_{air}'s of different crystals; the same is true for the differences between the initially observed crystal sizes; (5) the crystal size (D_{UHV}) distribution on the UHV cleaved surface differs from that (D_{air}) on the air cleaved surface with $\bar{D}_{UHV} > \bar{D}_{air}$; (6) the mean thickness $\bar{t}_{UHV}$ (or the total number Γ_{UHV} of condensed atoms) on the UHV cleaved surface is smaller than $\bar{t}_{air}$ (or Γ_{air}) on the air cleaved surface.

These observations will now be compared with theory. If condensation proceeds by nucleation--as it does in the temperature range considered here--then the total number $\Gamma(t)$ of atoms condensed after a deposition time t is given by

$$\Gamma(t) = \sum_i \int_{t'=0}^{t} n(\xi_i, t')\, g(\xi_i, t, t')\, dt' \quad . \qquad (1)$$

Here $n(\xi_i,t')$ is the number of crystals nucleated at the time t' with an orientation or kind of nucleation site (such as surface step, kink, hole, etc.), characterized by parameters ξ_i. $g(\xi_i,t,t') = \int_{t'}^{t} \frac{dg}{dt''}(\xi_i,t'')dt''$ is the number of atoms in the crystal at the time t, which grew from a nucleus, formed at time t'. The total number N(t') of crystals at time t' is determined by the nucleation rate $I(\xi_i,t)$ (as long as no coalescence has taken place):

$$N(t') = \sum_i \int_{t''=0}^{t'} n(\xi_i,t'')dt'' = \sum_i \int_{t''=0}^{t'} I(\xi_i,t'')(1 - F(t''))dt'' \quad , \quad (2)$$

where F(t'') is the fraction of the surface already covered by crystals (and their diffusion regions). Differences in $\Gamma(t)$ (observation 5) can therefore be due either to differences in the nucleation rate I or the growth rates as expressed by $\frac{dg}{dt''}$, or to both. That the nucleation rates differ is indicated by observation 3. However the growth rates may differ too. If the number of atoms hitting the growing crystal directly from the vapor phase is small compared to the number of atoms arriving at the crystal from the adsorption layer, then $\frac{dg}{dt''}$ is given by

$$\frac{dg}{dt''} = \frac{1}{4} \alpha \; s(g) \; a \; \beta \; N_i \; e^{\frac{\Delta G_a - \Delta G_A}{kT}} \quad . \quad (3)$$

Here α is the fraction of arriving atoms condensing on the crystal, s(g) is the circumference of the crystal, a is the distance of the potential minima for surface diffusion, β is the fraction of the number $N_i(cm^{-2}sec^{-1})$ of atoms incident onto the substrate which is adsorbed, ΔG_a (> 0) is the heat of adsorption and ΔG_D (> 0) is the activation energy for surface diffusion. For a crystal on the UHV cleaved surface to have a smaller $\frac{dg}{dt''}$

than that of a crystal with the same circumference on the air cleaved surface one of several of the following conditions must be fulfilled: (a) $\alpha_{UHV} < \alpha_{air}$, (b) $\beta_{UHV} < \beta_{air}$, (c) $(\Delta G_a - \Delta G_D)_{UHV} < (\Delta G_a - \Delta G_D)_{air}$, or (d) $T_{UHV} > T_{air}$. Unless the surface layer on the air cleaved surface reduces ΔG_D much more than ΔG_a it is difficult to see how condition (c) could be fulfilled. Conditions (a), (b), and (c) however could be fulfilled if it is assumed that a higher fraction $(1-\beta)$ of the atoms is reflected on the first encounter with the UHV cleaved surface and that the thermal accommodation of the hot vapor atom on the UHV cleaved surface is poorer than on the air cleaved surface. This would lead to a higher temperature of the Au (Ag, Al) adsorption layer ($T_{UHV} > T_{air}$) and very probably to a lower sticking coefficient ($\alpha_{UHV} < \alpha_{air}$). It seems therefore that the smaller amount of condensed material on the UHV cleaved surface as compared to the air cleaved surface can be attributed to a reduced growth rate only if a difference in β--which is usually taken to be 1--or in thermal accommodation is assumed.

However observation 3 suggests that mainly differences in I(t) are responsible for the differences in I'(t). In the phenomenological theory [18,20-22] the steady state nucleation rate for a nucleus consisting of g^* atoms with a square interface of edge length ℓ^* is given by

$$I = C_M C_L C_g C_Z \frac{a}{\nu} \ell^* \alpha\beta^2 N_i^2 \sqrt{-\frac{\left(\frac{\partial^2 \Delta G_K}{\partial g^2}\right)_{g=g^*}}{2\pi kT}} \; e^{-\frac{\Delta G_K(g^*) - 2\Delta G_a + \Delta G_D}{kT}} \quad . \quad (4)$$

The factors C_M, C_L, C_g take into account (a) the energy required to energize the subnuclear clusters in mobile adsorption layers (see e.g. ref. 21, p. 46), (b) the embryo distribution over the available surface sites in localized adsorption layers (see e.g. ref. 21, p. 45), and (c) the influence of embryos ($g > 1$) which is usually neglected (number of clusters consisting of g atoms $N_g << N_1$) [34]. C_Z is the Zeldovich factor, ν is the vibrational frequency of the adsorbed atoms, g^* is the number of atoms in the nucleus and

$$\Delta G_K(g) = g(\mu-\mu_a) + \phi_g + \phi_{gs} - \phi_{sg} \qquad (5)$$

is the Gibbs free energy of formation of an embryo or crystal at rest, consisting of g atoms. Here μ and μ_a are the chemical potentials of the atoms in the crystal and in the adsorption layer respectively, ϕ_g and ϕ_{gs} are the free surface and interfacial energies of the embryos or crystals of size g, and ϕ_{sg} is the free surface energy of the substrate area covered by the particle size g. In comparing equation (4) with experiment it has to be kept in mind that the observed quantity is not I but N as given by equation (2). In putting $N \sim I$ we have to make the assumption that the incubation period τ_i to establish the steady state nucleation rate is short compared to the total deposition time τ and that the coverage F during the film growth is always small ($F(t) << 1$). However observation 1 indicates that $\left(\frac{\tau_i}{\tau}\right)_{UHV} > \left(\frac{\tau_i}{\tau}\right)_{air}$ and Fig. 4a-c in Part I shows that only on the UHV cleaved surface is $F(\tau) << 1$. Nevertheless in all cases in which condensation took place on both surfaces was $\left(\frac{\tau_i}{\tau}\right) << 1$ ($\lesssim \frac{1}{10}$). Although the assumptions made above are fulfilled to different degrees on the air and UHV cleaved surfaces, the differences tend to compensate and we assume here that I is approximately proportional to N.

We now have to explain why $I_{air} > I_{UHV}$ in contradiction to theoretical expectations according to which impurities should reduce I (see ref. 21, p. 52 and 56). From Table 1, Part I, we obtain the following values for $kT \ln \frac{I_{air}}{I_{UHV}}$ (assuming full thermal accommodation of the adsorbed atom): .075, .085, .15, and .14 eV. From equation (4) we get $kT \ln \frac{I_{air}}{I_{UHV}} = kT \ln \frac{A_{air}}{A_{UHV}} + E_{UHV} - E_{air}$ where A is the pre-exponential and E the numerator of the (negative) exponential. If it is assumed that A is not very sensitive to the surface condition ($A_{air} \approx A_{UHV}$) then .075 eV $\lesssim E_{UHV} - E_{air} \lesssim$ .15 eV for the experiments of Table 1, Part I. The smaller value of $E = \Delta G_K(g^*) - 2\,\Delta G_a + \Delta G_D$ on the air cleaved surface in spite of the smaller expected value of ΔG_a (as compared to the UHV cleaved surface) can be easily accounted for by a smaller value of $\Delta G_K(g^*)$ (equation (5)) which contains the surface energy ϕ_g and interfacial energy ϕ_{gs}. The surface energy per Au atom in a large crystal is $\sigma_A^\infty \approx .65$ eV, in the somewhat unrealistic case of a crystal consisting of only a few atoms $\sigma_A^\circ \approx .22$ eV (according to the Tolman formula which is also not very realistic for such small particles). It is well known that the surface energy can be reduced easily by adsorption to one half or even a quarter of its value. If a small Au crystal is formed on an air cleaved alkali halide surface at a sufficiently high temperature the adsorbed species can diffuse onto the Au crystal and reduce its surface energy without a significant increase in the substrate surface energy. Also the interface energy can be reduced considerably if the lateral forces between the adsorbed species are weak as compared to those of the substrate atoms and if the adsorbed species is at least partially incorporated into the interface. This results in a

considerable reduction of the interface shear modulus and therefore of the interface energy in van der Merwe's interface model [35]. In a "crystal" consisting of say, 5 or more atoms, $\Delta G_K(g^*)$ can therefore easily be reduced by .5 eV or more. On the other hand the heat of adsorption ΔG_a of Au on a surface covered with impurities is expected to be lower than on the clean surface. A value of $\Delta G_a > .4$ eV per atom is necessary in order to obtain a collision rate high enough for nucleation to become possible under the experimental conditions of I. If ΔG_a would be reduced considerably by adsorption, e.g. to half its value, the number of adsorbed atoms on the air cleaved surface would become so small, that the nucleation rate would become negligible in contradiction to experiment. Higher values than $\Delta G_a \approx 1$ eV for the clean surface are unlikely so that we can conclude that impurities cannot decrease ΔG_a by more than several tenths of an eV per atom. Inasmuch as ΔG_D is usually small compared to ΔG_a and $\Delta G_K(g^*)$, the decrease from E_{UHV} to E_{air} due to impurity adsorption by .075 - .15 eV is quite plausible, if the nuclei are assumed to consist of only a few atoms or if only a small reduction of the surface energy occurs upon impurity adsorption on larger nuclei. However it has to be kept in mind that the pre-exponential may also vary considerably with surface condition. The largest uncertainty probably is in the Lothe-Pound factor C_M in equation (4), the magnitude of which is still a matter of dispute [36]. This factor can change I by many orders of magnitude depending upon the mobility of the subnuclear clusters, which may differ considerably between UHV and air cleaved surfaces. The phenomenological theory thus can explain the higher total condensation coefficient and particle density on the air-cleaved surface but allows no reliable conclusions at present because of the large

number of poorly understood variables (e.g. C_M, C_g, α, β, etc.) which it contains.

The atomistic theory [23] on the other hand contains only a few variables, but cannot explain in its present form the observations considered here. The nucleation rate is given by

$$I = N_i N_o a^2 \left(\frac{1}{\nu}\frac{N_i}{N_o}\right)^{g^*} e^{\frac{E_{g^*} + (g^*+1)\Delta G_a - \Delta G_D}{kT}} \qquad (6)$$

where the symbols have the same significance as in equations (4) and (5), N_o is the density of adsorption sites and E_{g^*} is the energy of dissociation of the critical nucleus. A comparison of the exponents in equations (4) and (6) shows that $\Delta G_K(g^*) = -[E_{g^*} + (g^*-1)\Delta G_a] \leq 0$, i.e. in the atomistic theory the quantity corresponding to the Gibbs free energy of formation of a nucleus is negative, i.e. there is no nucleation barrier and the term "nucleus" as that particle which has equal probability for growth and decay loses its meaning. The single atom becomes a "nucleus" and the only way it can "decay" is by desorption, so that the heat of adsorption ΔG_a becomes the parameter decisive for the nucleation rate. This is also true if the "nucleus" consists of two or more atoms, because such a nucleus is formed by collision of single atoms--except in systems which already contain in the vapor phase diatomic molecules such as Ag and Au--so that a sufficiently high ΔG_a is necessary in order to have enough collisions between atoms and subnuclear clusters (i.e. other atoms, diatomic and polyatomic molecules). If ΔG_a is decreased by surface impurities as generally assumed, then the "nucleation rate" will decrease in contradiction to experiment (see above). The reason why I can increase

in the phenomenological theory in spite of a decreased ΔG_a is that the magnitude of the positive terms ϕ_g and ϕ_{gs} in $\Delta G_K(g^*)$ (equation (5)) are reduced by impurities. If, however, ΔG_a is assumed to be increased by surface impurities, the atomistic theory can also account for the observations on air and UHV cleaved surfaces. This could happen if the Au atoms penetrate into the impurity layer so that they are bound normally just as on the clean alkali halide surface and, in addition, laterally to the adsorbed species. In this model, in which the metal atoms diffuse <u>in</u> the impurity layer and not on top of it, ΔG_D is expected to be considerably higher than on the clean surface and may partially compensate the increase of ΔG_a.

Just the opposite is the case in Harsdorff's model [5] of the influence of surface layers on the growth of metal films on alkali halides. Here the metal atoms are adsorbed on top of an adsorbed multilayer--assumed to consist of H_2O on air cleaved alkali halides--which themselves are so weakly bound to the alkali halide surface that they can be desorbed successively by heating to several 100°C in vacuum. Under the conditions of the Au experiments of Table 1 in Part I the surface should be covered by three water layers. These layers are assumed to reduce the activation energy for surface diffusion ΔG_D--which plays the central role in Harsdorff's model--and therefore according to equation (4) or (6) to increase the nucleation rate. This conclusion however neglects the relation between ΔG_a and ΔG_D. It is generally assumed that $\Delta G_D \approx \frac{1}{5}$ to $\frac{1}{10}\,\Delta G_a$. A change of ΔG_D is therefore accompanied by a much larger change of ΔG_a which overcompensates the ΔG_D change and leads to a reduction of I according to equations (4) and (6) in contradiction to experiment.

In conclusion, the differences in the number of condensed atoms Γ and nucleation rates I between substrates with different surface condition can in principle be explained by differences in $\Delta G_K(g^*)$, ΔG_a or ΔG_D. The explanation in terms of $\Delta G_K(g^*)$ appears the most realistic, but only if one of the following conditions is fulfilled: (a) the nuclei are very small ($g^* \approx 5$-10), (b) the decrease of the "surface energy" and "interfacial energy" due to impurities is very small, or (c) the subnuclear clusters are mobile to different degrees depending upon surface condition. The last condition involves major differences in the pre-exponential in addition to differences in $\Delta G_K(g^*)$.

2.3. Film orientation and orientation perfection

The most important quantity in the context of this paper is not the number of crystals in the film, but their orientation and the perfection of orientation. The following experimental results of Part I have to be compared with theory: (1) The thinnest films of Au on NaCl and KCl have predominantly (100) orientation in the temperature range investigated irrespective of substrate surface condition. (2) In addition to this predominant orientation several other weak orientations are observed. (3) The azimuthal alignment of the crystals is poor in the thinnest films and increases with film thickness (particle size). (4) The azimuthal alignment is better on UHV cleaved surfaces with large particle size than on air cleaved surfaces (small particle size), but seems to become independent of the surface condition once the particle sizes are comparable. (5) Ag on KCl and Al on NaCl, in contrast to Au on NaCl and KCl, have under similar conditions not only prominent (100) but also prominent (111)

orientations, with weak subsidiary orientations, appearing in the earliest stages of film growth. (6) The crystals are always well aligned with respect to the substrate normal under the experimental conditions of Part I.

In the phenomenological nucleation theory the formation of epitaxial nuclei is attributed to the orientation dependence of the interfacial free energy [17,18] (see also refs. 20, p. 493; 21, p. 69; 22, p. 18). For every minimum ϕ_{gs}^{M} (θ_M, ϕ_M) of the interfacial energy equations (4) and (5) predict a maximum I_M (θ_M, ϕ_M) of the nucleation rate. The relative nucleation rates for the different orientations with minimal interfacial energies depend upon the depth of the minima while the perfection of the orientations depends upon the sharpness of the minima. If interpreted this way, the observations, (1)-(6) above, indicate that for Au, Ag, and Al on NaCl and KCl there are several minima of ϕ_{gs}, with the (100) minimum by far the lowest in Au and the (100) and the (111)[011] minima about equally deep in Ag and Al. The poor azimuthal alignment in the thinnest films indicates that the minima are poorly pronounced. For the interpretation of the weak subsidiary orientations ((100), (211)[001] as defined in Part I.3.1.) in this manner it has to be assumed that these crystals really have direct contact with the substrate and are not oriented overgrowth of Au on Au as suggested by Göttsche [37] who found the same orientations in films which were deposited at room temperature in ordinary vacuum and annealed afterwards. This assumption appears justified on the basis of the correlation between TED and TEM results (see Part I.3.5.). Another possible interpretation is in terms of the multiple twin model which has been convincingly demonstrated by Ino [38] for predominantly (111) oriented Au films. However it can also be excluded--except for the (211)[011] orientations--because of the disagreement between the observed and calculated spot position and intensities,

both for base crystals with (111) and (100) orientations. Table 2 gives the orientation relationships of the primary and secondary twins for which the expected diffraction patterns have been determined. The equivalent twins are obtained from those listed by proper permutations and sign changes of the indices. An argument against a possible interpretation of the (211)[011] orientations in terms of the multiple twinning model as upper secondary twins of the (100) orientation is the observation of the (211)[011] orientations in Al films, in which no multiple twinning would be expected because of the high stacking fault energy of Al.

The indexing chosen in Part I can explain all relevant diffraction features. The calculated pattern of one of the orientations--the four equivalent (110) orientations defined in Part I. 3.1.--which accounts for most of the weak subsidiary spots in very thin films is shown in Fig. 1. It has to be pointed out however that the interpretation may not be unique because it is based on only one reciprocal lattice section and on the combination of TED and bright field TEM. For instance, a different interpretation for apparently the same TED pattern of thin Au films deposited on vacuum cleaved NaCl in ordinary vacuum at 300°C has been given recently [39], but the data reported in Part I definitely do not fit this interpretation. Differences in interpretation alone however cannot account for the discrepancies between recent investigations, especially between those reported in Part I and Ino's [38], which must be attributed to differences in experimental conditions. The most important difference is probably in the annealing of the films: in Ino's setup [4,38] the crystals cool only about 10°C within 10 min or more, while in our setup

(see Part I. 2.) the temperature drops about 150°C within the first 10 min. Considerable annealing, which leads to coalescence and to secondary orientations (see Part I. 3.4.3. and II. 3.2.), is therefore likely to have occurred in Ino's work [38], but not in ours. This is in contradiction to Ino's suggestion that the crystals which are multiply twinned with respect to crystals with (111) base orientations are formed by nucleation and not by coalescence. According to our experience with wedge films, even Ino's thinnest films (Fig. 18a in ref. 38) show coalescence. Even if the films are quenched immediately after deposition it is difficult to exclude coalescence completely, at least in slow depositions, because it occurs to a small degree simultaneously with nucleation and growth. Until disproven, the orientations reported in Part I will be considered not to be due to coalescence.

The interpretation in terms of nucleation as briefly discussed above has the following difficulties: (1) In order to explain the high nucleation rates observed very large values of $\mu_a - \mu$ in equations (4) and (5) have to be assumed, which lead according to the Gibbs-Thomson equation to very small g^* (< 10), unless the pre-exponential factors are assumed to be very large. (2) The difference between the partical numbers on air and UHV cleaved surfaces suggest also a very small nucleus size unless large differences in the pre-exponential factors compensate for the differences in $\Delta G_K(g^*)$ (see 2.2.). (3) The pre-exponential in the present formula for the nucleation rate (equation (4)) can be sufficiently large and change strongly with surface condition only if the nuclei and subnuclear clusters are mobile (Lothe-Pound factor C_M). Mobility is also expected if g^* is small, if the activation energy for surface

diffusion is small. If the mobility includes rotation of the "crystals" no orientation dependent "interfacial energy" can be ascribed to them and no epitaxial nucleation is to be expected. The formation of preferred orientations has then to be ascribed to the growth of the crystals from the nuclei. This is governed by essentially the same extremum conditions as nucleation (see e.g. ref. 40, equations (6) and (7)): the Gibbs free energy G of the system has to be an extremum, for nucleation G--or more precisely its change ΔG upon nucleation--has to be a maximum (Fig. 2b), in the case considered here G has to be a minimum (Fig. 2c). As long as the activation barrier for a crystal to reach the configuration of minimum G is not too high the minimization of the interfacial energy will lead to epitaxy by growth in the same manner as it does by nucleation of nuclei which are large enough and do not rotate. In terms of the schematical $\Delta G(g)$ diagram (Fig. 2) the difference between the epitaxial nucleation model and the epitaxial growth model can be described as follows: in the nucleation model (Fig. 2b), the interfacial energy ϕ_{gs} and therefore $\Delta G_K(g)$ (equation (5)) varies strongly with crystal orientation (θ,ϕ) and consequently according to the Thomson-Gibbs equation also g^* and according to equation (4) the nucleation rate. Nuclei with orientations (θ_M,ϕ_M) corresponding to minima of the "interfacial energy" will be formed at a much higher rate than nuclei with other orientations (θ_i,ϕ_i). In the growth model (Fig. 2d) the variation of the "interfacial energy" with orientation is very small--if it can be defined at all--and all orientations are formed with comparable probability. With increasing interface size the minima (θ_M,ϕ_M) of the interfacial energy become more pronounced and crystals with an orientation θ_M,ϕ_M grow preferentially or crystals

with different orientations θ_i, ϕ_i rotate into orientation θ_M, ϕ_M. While the basic assumption of the growth model, that the orientation of the nuclei may be very poor, cannot be examined presently because of the small size of the nuclei, observations 3 and 4 (see above) which are in agreement with Matthews' observations [14,32] strongly favor such an interpretation.

The growth model is diametrically opposed to Walton's model [23] of the mechanism of epitaxy. In his model the crystal orientation is determined by the orientation of the "nucleus" consisting in general of 2-4 atoms. Actually there is no nucleus because the addition of an atom to a cluster of arbitrary size is accompanied with an energy gain, so that no maximum in ΔG is formed as suggested by the word nucleus (Fig. 2a); rather ΔG decreases continuously with g as shown schematically in Fig. 2c. The tendency of the 2 to 4 atoms in the "nucleus" to lie in the potential minima of the surface determines the orientation of the cluster which is maintained upon its further growth. This is in disagreement with observations 3 and 4. Observation 5 cannot be explained either as the following consideration shows: Walton's model asserts that if the nucleus is a diatomic molecule ("twin") a (111) orientation is predicted and if it consists of three atoms a (100) orientation should be formed. The larger the binding energy E_2 of the diatomic molecule, the higher the probability that the "twin" is already the nucleus and that a (111) orientation is formed. Therefore Au with $E_2 = 2.23 \pm .10$ eV [41] should show a stronger tendency to form (111) oriented nuclei than Ag with $E_2 = 1.63 \pm .10$ eV [41] or Al for which no diatomic molecules have been detected to date, in contradiction to experiment (observation 5). Another argument against Walton's

epitaxy model is that many f.c.c. metals show (100) epitaxy on all alkali halides from LiF to KI with widely differing distances between the potential minima in the surface; obviously the orientation of a given cluster configuration should change with the substrate lattice parameter. These difficulties of Walton's epitaxy model do not mean that atomic theories of condensation such as Zinsmeister's [42] cannot account for epitaxy. They only indicate that the orientation is not determined by that of the smallest stable cluster but develops in the later stages of its growth.

The observations are also incompatible with Harsdorff's model [5] of the influence of surface layers on the perfection of the orientation. According to his model the orientation should be more perfect on an air cleaved surface than on a UHV cleaved surface which is in contradiction to experiment (observation 4, see also refs. 12, 14).

In conclusion, while within the framework of the phenomenological nucleation theory the orientations observed in very thin films can in principle be attributed to epitaxial nucleation, the orientations suggest that the nuclei are only poorly oriented and that the well defined orientations are formed in the growth process by the tendency to be in the state of minimum Gibbs free energy which depends upon interfacial energy and its orientation dependence.

2.4. Residual gas influence

The experiments described in Part I were performed in UHV and the influence of the residual gas is considered to be negligible. However in experiments in ordinary vacuum [4,8,9] a strong influence of the residual gas was noted. This was explained in terms of the influence of

residual gases on the activation energy for surface diffusion ΔG_D (or "place exchange energy") [8]. However residual gases influence also the free energy of formation of a nucleus $\Delta G_K(g^*)$, the heat of adsorption ΔG_a of the metal atoms on the surface, the pre-exponential factor in the nucleation rate (equation (4)) and the nucleus size g^*. As discussed in II.2.2 and II.2.3. $\Delta G_K(g^*)$ is the most probable quantity responsible for the dependence of I on the surface condition. This suggests explanation of the residual gas influence also in terms of $\Delta G_K(g^*)$.

If an alkali halide surface is cleaved in an active residual gas and the evaporation is performed in it, the gas is adsorbed on the substrate surface and on the surface of the clusters and crystals of the condensing material. It is obvious that the nature and thickness of the adsorption layer on a given surface will depend on the pressure and nature of the residual gas, and the surface temperature. Furthermore, on a vacuum cleaved substrate surface it will depend on the exposure time prior to deposition, and on the surface of the growing clusters and crystals it will depend on the rate at which the surface area increases, which is to a large extent determined by the deposition rate. These adsorption layers influence $\Delta G_K(g^*)$, ΔG_a, ΔG_D and other quantities on which the nucleus size g^* (Thomson-Gibbs equation), the nucleation rate I (equation (4)), and the growth rate (equation (3)) depend; as discussed in II.2.2. adsorption is expected to decrease g^*, $\Delta G_K(g^*)$, ΔG_a, and ΔG_D, but the decrease of $\Delta G_K(g^*) + \Delta G_D$ overcompensates that of ΔG_a so that I increases. The magnitude of the increase of I depends on the magnitude of the decrease of the "surface" and "interfacial free energies" ϕ_g and ϕ_{gs} due to adsorption which in turn depends on the rate at which gas is supplied to the

growing surface. If the surface grows sufficiently slowly so that many residual gas atoms (or molecules) can be adsorbed, ϕ_g for a given particle size g will be reduced more than in the case where the surface area increases so rapidly that only a small fraction of it is covered with adsorbed atoms. This can explain qualitatively the observation of Adamsky and LeBlanc [30] that the nucleation rate I of Au on vacuum cleaved NaCl at 300°C in the 10^{-6} torr range increases with decreasing deposition rate N_i in contradiction to nucleation theory (equation (4)) neglecting the residual gas influence. (It should be noted that this explanation is valid only if the surface energy of the crystal is much larger than that of the substrate.) I will increase with decreasing N_i until the surface of the growing cluster is covered with a saturated adsorption layer. This critical deposition rate N_i will depend on the pressure p_r of the residual gas, its nature, which determines the heat of adsorption ΔG_a^C on the cluster surface, and on the temperature T of the cluster. Any further decrease of N_i (or at constant N_i any further increase in residual gas pressure) will not reduce ϕ_g for a given g any further and I will start to decrease as expected from nucleation theory neglecting the residual gas influence.

If the observed influence of the residual gas on the orientation perfection [8] is to be attributed to the nucleation and initial growth stage, the assumption has to be made that in the presence of active residual gases the processes taking place in the later stages of the film growth (coalescence and filling-in) do not significantly influence the orientation perfection in contrast to the UHV results described in Part I. This assumption is necessary because the films studied were in general 450 Å thick,

and even the thinnest film for which this residual gas influence was checked was 30 Å thick, a thickness at which massive contact between the crystals must have already taken place at the substrate temperature and deposition rate used (60°C and 1 Å/sec). There is considerable evidence that coalescence takes place also in f.c.c. metal films deposited in normal vacuum onto alkali halides [3]. We consider it therefore as premature to speculate on the origin of the influence of the residual gas on the orientation perfection, although the suggested explanation in terms of ΔG_D seems unlikely to us on the basis of the arguments given in II.2.2. and II.2.3., and although an explanation in terms of the influence of the residual gas on ϕ_g and ϕ_{gs} (and therefore on $\Delta G_K(g^*)$ could be offered along the lines discussed in II.2.2. and II.2.3.

3. Coalescence State

3.1. Number and size of crystals

Coalescence can occur in any stage of the film growth and reduce the number of crystals and change their orientation. It becomes a major factor when the particle density N is so high that the mean particle size is comparable with the mean particle distance. With increasing particle density more and more crystals touch each other and coalesce so that the particle density increases at a decreasing rate until it reaches a maximum N_{max} at a time t_{max} after which coalescence overcompensates nucleation leading to a decrease of N. The beginning of the coalescence stage can be (arbitrarily) identified as that time $t_c < t_{max}$ at which $N = N_c = \frac{1}{2} N_{max}$. Although the mean particle size increases upon coalescence, the area $\frac{F}{N}$ per coalesced particle is in general smaller than the

sum of the areas of the particles from which it was formed. This shows that coalescence is accompanied by a decrease in average surface to volume ratio of the particles which points to the cause of coalescence. The system tries to minimize its Gibbs free energy by reducing the surface free energy ϕ_g of the particles. The possible mechanisms involved in this minimization process have been discussed by Pashley et al. [43]. We are concerned here only with the driving force for the process, the Gibbs free surface energy ϕ_g, and the influence of the nature and condition of the substrate surface and of residual gas on ϕ_g. If the particles have different orientations (θ_i, ϕ_i) before coalescence occurs, the inter-particle interfacial free energy $\phi_{gg'}^{ik}$, becomes an important part of the energy balance which determines the minimum free energy configuration after coalescence. Under certain conditions (see 3.2.) the particle resulting from the coalescence of differently oriented crystals is not a single crystal but consists of parts with different orientations. As the results concerning the film structure in the coalescence stage described in Part I were not concerned with particle number and size, but only with particle orientation and particle shape, we will limit the discussion to the latter two quantities.

3.2. Orientation, orientation perfection and shape of crystals

The following observations reported in Part I have to be accounted for: (1) In Au films on air cleaved NaCl, UHV and air cleaved KCl coalescence leads to the elimination of the (111) oriented crystals and of all other crystals having an orientation different from the (100) orientation. Simultaneously the crystal habit changes from {111} habit to a {100} habit

which is accompanied by the formation of a surface layer on the ⟨100⟩ surfaces with a periodicity in the {011} direction of approximately 5/3 of the Au periodicity in this direction. (2) In Au films on UHV cleaved NaCl and in Ag films on UHV and air cleaved KCl coalescence leads to approximate $(211)_{111}$ orientations. (3) In Al films on NaCl the (111) orientations increase on coalescence at the expense of the (100) orientation with a simultaneous decrease of the orientation perfection and of the {100} facets which are replaced by (111) planes parallel to the substrate. We consider here only the coalescence of (100) and (111) oriented crystals of comparable sizes g and g'. As suggested in 3.1., the coalescence process is determined by the surface and interfacial free energies. Consider two crystals consisting of g and g' atoms with orientations (θ_i,ϕ_i) and (θ_k,ϕ_k) respectively. Then the Gibbs free energy change upon coalescence is

$$\Delta G = \phi^{ik}_{gg'} + \phi^{ik}_{g+g'} + \phi^{ik}_{g+g',s} - \phi^{ik}_{s,g+g'} - \left(\phi^{i}_{g} + \phi^{k}_{g'} + \phi^{i}_{gs} + \phi^{k}_{gs} - \phi^{i}_{sg} - \phi^{k}_{sg}\right). \quad (7)$$

Here each ϕ is given by an expression of the form $\phi = \sum \sigma_{hkl}F_{hkl}$ where the σ_{hkl} are the specific free surface (or interface) energy of the various particle surfaces (or interfaces) with areas F_{hkl}. In order for coalescence to occur we must have $\Delta G<0$ and the activation energy to reach a state with lower Gibbs free energy G must be sufficiently low. This state of lower $G = G_M$ is not necessarily that of lowest G, because there can be several minima of G separated from the original state by activation barriers of different height. If the coalescing crystals have the same orientation and no reaction takes place during coalescence which changes the specific free surface and interface energies of the different faces of the crystal and of the interface with the substrate, there is no motivation for a major

change in orientation and the result of coalescence is only an increase in particle size, provided that the state with $G = G_M$ can be reached (Wulff's law). However when the orientations of the coalescing particles differ and/or when reaction--involving the residual gas or the substrate--occurs, considerable changes in particle orientation and/or shape can take place. A general discussion of these changes on the basis of equation (7) is too complex. We consider here therefore only the cases studied in Part I.

In order to understand observation 1 (Au on air cleaved NaCl, UHV and air cleaved KCl) one has to take into account that Au forms compounds with the alkali metals. Low energy electron diffraction has shown [44] that a {100} Au surface which was cleaned by ion combardment develops a complex surface structure ascribed to a gold-alkali compound; no such surface structure is formed under identical conditions on a {111} surface [45]. Unless a gold-alkali compound layer with the same lateral periodicity as that of the Au {111} plane is formed on the Au {111} surface these observations suggest that a {100} surface can reduce its free surface energy σ_{100} by forming a reaction layer, while a {111} surface cannot. Although the reaction layer on the {100} surface disorders (reversibly) at 800°C it cannot be removed by heating to the melting point. When two Au crystals coalesce a considerable amount of energy can be liberated due to the reduction of the surface to volume ratio. For example, if two spherical particles of 100 Å radius coalesce to form one spherical particle, $4.7 \cdot 10^3$ eV are liberated assuming a specific free energy of 1500 erg/cm^2. The liberated energy--or part of it--can initiate an exothermic reaction between Au and the substrate. This reaction may not only produce the reaction layer

on the {100} surface reducing σ_{100}, but may also liberate additional energy aiding in the atomic rearrangement during coalescence. If the specific free surface energy $\sigma_{100}^{R.L.}$ of the Au {100} surface covered with the reaction layer is lower than σ_{111}, then a {100} habit minimizes G-- or maximizes $|\Delta G|$--. If in addition the specific free interfacial energies σ_{hkl}^{i} are not changed in such a manner that $\sigma_{111}^{i} < \sigma_{100}^{i}$, then the (100) orientation is the favored coalescence orientation. If this explanation is accepted it has to be concluded that the tendency for the formation of this orientation varies with the kind and condition of the substrate surface. The observation that on air cleaved, i.e. hydrated, NaCl the reaction layer is formed but not on UHV cleaved NaCl suggests that the activation energy needed to start the reaction is mainly responsible for this dependence. This is supported by the much stronger tendency for reaction on KI than on KCl which has a higher lattice energy.

Certain features in the RED patterns discussed in Part I, such as streaked reflections not normal to the surface indicate that the absorption of the (111) oriented crystals by the (100) oriented crystals involves intermediate stages like twinning, but the diffraction pattern due to the surface layer is so strong that a detailed evaluation of these features was not possible. This is not true in observation 2 (Au on UHV cleaved NaCl, Ag on air and UHV cleaved KCl), where complex orientations due to coalescence between (100) and (111) oriented crystals are clearly noticeable. The interpretation of these orientations is based on the following assumptions: (1) no reaction takes place with the substrate during coalescence so that $\sigma_{111} < \sigma_{100}$; (2) the specific free twin boundary energy σ_T is a very small fraction of the specific free surface energy.

As a consequence of (1) the coalesced particles tend to be bound by {111} planes like the crystals before coalescence. As a consequence of (2) particle agglomerates may be formed in which the individual parts are in twin positions relative to each other, if this so-called multiple twinning process is accompanied with a decrease in G, say to G_M. As twinning is a diffusionless transformation, little activation energy is needed for this process so that it occurs spontaneously. The multiple twin configuration may not be the configuration of the particle aggregate with lowest G. The state of lowest $G = G_{MM}$ is expected to be a single crystal bounded by {100} and {111} planes if the difference between σ_{100} and σ_{111} is as small as generally accepted ($\sigma_{100}:\sigma_{111} = 1.1$ [46]), if the specific free twin boundary energies are assumed to be twice the stacking fault energies ($\gamma_{Ag} = 21$ erg/cm^2 and $\gamma_{Au} = 52$ erg/cm^2 [47]) and if small deviations from the exact twin orientations are neglected. The state with $G = G_{MM}$ can in principal be reached diffusionless by migration of the several twin boundaries through the crystal. However, simultaneously the minimum free surface energy configuration has to be maintained which requires considerable diffusion. This is associated with an activation energy so that it can be reached only after a long period compared to the twinning process, at higher temperature or when assisted by some energy source such as an exothermic reaction with the substrate (see above). Multiple twinning in films of f.c.c. metals on alkali halides was first suggested by Menzer [48] to explain the epitaxy of Ag on NaCl. It has been discounted in many experiments on the nucleation of f.c.c. metals on alkali halides, revived by Goswami [49] to explain the (211) orientation of Ag films on NaCl, and discounted by Göttsche [37] on the basis of the argument that double twinning

leads to a (744) orientation which deviates from the (211) orientation in the ⟨011⟩ azimuth by 3.6°. Recently, however, Ino [38] has clearly demonstrated the existence of multiple twinning in Au films on NaCl using TED and bright and dark field TEM. His films differ from ours in that in his case the fraction of crystals with (100) orientation is very small with most of the crystals multiply twinned with respect to base crystals with (111) orientations, while in our case (see Part I) the (100) orientation is generally stronger which suggests that most of the crystals are double twinned with respect to base crystals in (100) orientation. On the basis of the observations on the influence of annealing on the film structure (Part I.3.4.3.), we attribute the differences mainly to strong annealing effects in Ino's Au films.

The (approximate) (211) orientation has also been observed by Kehoe [50] in Cu films on NaCl, KCl, KBr, and KI, Ag films on NaCl and KBr and Au films on NaCl deposited slowly in ordinary vacuum on air cleaved surfaces. Slow deposition allows coalescence processes to occur during film growth so that Kehoe's (211) orientation is probably also a coalescence orientation. This was already suggested by Matthews et al. [32], who accepted Göttsche's [37] model of the (211) orientation: a Au crystal grows with its (110) plane parallel to the (111) plane of a (100) oriented crystal; this could happen during coalescence if the interfacial energy of the (110)(111) grain boundary is very low, which is unlikely. We suggest an interpretation in terms of multiple twinning which is based on the observation that the approximate (211) orientation is neither precisely a (211) nor (744) orientation but is roughly halfway between both orientations. Table 2 indicates that the plane in the upper secondary twin ((100)-$T2_u$) of a (100) oriented

crystal which is parallel to the substrate is a $(\bar{7}44)$ plane, and similarly that of a (111) oriented crystal ((111)-$T2_u$) is a $(\bar{7},5,13)$ plane. Both secondary twins have a common $[\bar{8}7\bar{7}]$ axis which deviates from the $[\bar{1}1\bar{1}]$ axis by 3°40'. The $[\bar{7}44]$ direction in the (111)-$T2_u$ twin makes an angle of 54°44' = 60°-5°16' with its $[\bar{7},5,13]$ direction. A 60° rotation of part of a crystal about its $[\bar{1}1\bar{1}]$ axis brings that part of the crystal into twin position with respect to the rest of the crystal. The secondary twins, (100)-$T2_u$ and (111)-$T2_u$ are therefore nearly in twin position relative to each other, with misorientations of several degrees which are of the same magnitude as those required in Ino's multiple twin model. Thus five approximate twin boundaries with known low interfacial energy can mediate between the (100) and (111)[011] orientation. When crystals with such orientations coalesce, this multiply twinned structure is likely to be formed. The small misorientation may be accommodated in several ways, depending upon experimental conditions, which could account for the slight orientation differences between the results of Part I and others [37,49,50] and for the details in the RED patterns (spot shapes) which require further study. It should be pointed out that the TED observations of Matthews [14] if properly interpreted agree also with the TED and RED results of Part I. Matthews has attributed the strong spots or arcs observed in the coalescence stage on the (111) ring to single twinning. As Fig. 3 indicates very strong misorientations have to be assumed to observe these spots which is in contradiction to their high intensity. However double twinning with the resulting approximate (211) orientation can easily account for the spots. Therefore Matthews' observations also indicate that the disappearance of the (100)

orientation in Au films on UHV cleaved NaCl upon coalescence is not simple due to a growth of the (111) oriented crystal at the expense of the (100) oriented crystals, but proceeds via a complex transition stage which can be explained in terms of multiple twinning. Matthews' hypothesis that the difference in particle numbers at the time of coalescence is responsible for whether the film will assume a (100) or a (111) orientation also is not tenable on the basis of the comparison of Au on UHV cleaved NaCl and KCl: In both cases a (111) orientation should be formed because of the small particle number in contradiction to experiment. The difference between films on NaCl and KCl can however be easily accounted for by the observation that no reaction takes place between Au and UHV cleaved NaCl. The observation of Ino et al. [4] that there is no difference between Au films grown on UHV and air cleaved surfaces is due to their strong bake-out which removes the hydrated surface layer (see I.3.4.1.). The importance of the hydrated surface layer has also been well established for Ag on NaCl by Bethge et al. [13].

The third observation (Al/NaCl) concerns a case in which there is no indication for a reaction between film and substrate material upon coalescence and in which the twin boundary energy σ_T is not small compared to the surface energy (stacking fault energy $\gamma = 280$ erg/cm^2; estimated surface energy $\sigma \approx 1000$ erg/cm^2). Because of the high γ there are no aggregate configurations of coalesced (100) and (111) oriented crystals with low G. Therefore the coalesced particle has to assume either fully a (111) or a (100) orientation in order to eliminate high energy interfaces. The observation that the (111) orientation is preferred under the experimental conditions of Part I irrespective of the substrate surface condition indicates

that σ_{100} is sufficiently larger than σ_{111} in order to make a crystal bounded mainly by {111} planes more stable than one bounded equally by {100} and {111} planes.

In conclusion, the three metals on the few substrates investigated display strongly differing coalescence behavior: (1) reaction with the substrate resulting in changes of the surface free energies σ_{hkl} of the metals due to formation of surface layers, (2) multiple twinning to eliminate high energy grain boundaries in coalesced crystals with different orientation, and (3) annihilation of one orientation upon coalescence of crystals with different orientation without formation of stable or metastable twin boundaries. The details of these processes still need to be investigated and others may be found in other systems.

3.3. Residual Gas Influence on Coalescence

The results of Kehoe [50] for Cu, Ag, and Au deposited in ordinary vacuum on alkali halide surfaces cleaved in air and those of Gillet et al.[39] for Au deposited in ordinary vacuum onto vacuum cleaved NaCl clearly indicate that type 2 coalescence involving multiple twinning occurs also in the presence of residual gases. Kehoe's data indicate furthermore that up to 230°C the type 1 coalescence mechanism does not occur in Au films on air cleaved NaCl, probably because the temperature is too low for the reaction to occur. While these results indicate that the residual gases usually present in ordinary vacuum systems have little influence on the coalescence process, those of Harsdorff et al. [8] however show the contrary: If it is assumed that the orientation perfection is determined by the nucleation and initial growth process (II.2.3.) then the residual gases present in their

experiment must suppress coalescence. The same assumption must be made if the temperature dependence of the orientation perfection [5] is to be attributed to nucleation as suggested [5] or to initial growth. Such an assumption does not appear unreasonable in view of the observation that deposition in weakly adsorbed gases (H_2, He) leads to very poor orientation which could be due to coalescence of well oriented crystals with different orientations like in UHV. For a discussion of the experiments on the orientation perfection see ref. [12].

4. Filling-in Stage

The filling-in stage is characterized by the filling-in of the space between the coalesced crystals, partially by their lateral growth, partially by nucleation and growth of small crystals between the large coalesced crystals and their subsequent coalescence upon contact with the larger crystals. As a consequence of these processes large flat crystals are formed which grow laterally to join up into a network of crystals. Further lateral growth leads to formation of channels, holes, and finally to a continuous film (see e.g. Fig. 11 c-e, h-k in ref. [12]). The processes which determine the orientation of the continuous film start at the beginning of the filling-in stage when the crystals with large lateral dimensions are formed. The following observations are to be explained: (1) the crystals are plate-like instead of sphere-like; (2) in some cases the (111) orientation and other orientations disappear completely and only the (100) orientation is left, in others the (100) orientation and the approximate (211) coalescence orientations disappear and only the (111) orientations are left. Observation 1 can be due to two causes: either the

activation energy needed for the considerable material transport required to form a particle with minimum surface to volume ratio (i.e. a polyhedron approximating a sphere) is missing or the plate-like habit represents a lower free energy configuration. Applying Wulff's law (for its validity, see e.g. ref. [40]) it can be shown easily that the ratio of the surface energy ϕ_1 of a spherical particle to that of (ϕ_2) a rectangular particle of minimum free energy configuration and identical volume is given by

$$\phi_1/\phi_2 = \left(\frac{\pi}{3}\right)^{2/3} \frac{1}{\left(1 + \frac{\sigma_i}{\sigma}\right)^{2/3}} + \frac{\sigma_s}{\sigma} \frac{1}{1 + \frac{\sigma_i}{\sigma}} \quad . \tag{8}$$

Here σ, σ_i, σ_s are the (size and shape independent) specific free surface energies of the free surface of the crystal, its interface with the substrate, and of the substrate respectively. For Au on NaCl and KCl $\sigma_s/\sigma \approx 1/10$ and $\phi_1 > \phi_2$ only if $\sigma_i \lesssim 1/5\ \sigma$, i.e. the spherical crystal has a higher free energy if the $\sigma_i \lesssim 1/5\ \sigma \approx 300$ erg/cm^2. Although such low values of the interfacial energy seem possible, it is likely that the formation of the plate-like crystals is mainly due to the first cause.

The second observation has doubtlessly to be attributed to the minimization of the free energy of the plate-like crystal aggregate by acquiring the same low energy external surface parallel to the substrate ({100} or {111}) over the whole aggregate and by eliminating twin boundaries, which can easily move through the crystal. In cases where a {100} free substrate surface is favored (reduction of σ_{100} by a reaction layer) the free surface favors a motion of the twin boundaries from the (100) oriented part of the crystal to the other parts whereby the whole aggregate acquires a (100) orientation. In the cases where a {111} free surface is favored (no reduction of σ_{100} by a reaction layer) twin boundary motion away from the

(111) oriented part of the aggregate will occur thus eliminating all twins--and with it the approximate (211) orientations and transforming the whole aggregate into a (111) oriented crystal. However many twin boundaries and microtwins will still persist to accommodate the azimuthal orientation difference between the various (111) orientations and to accommodate the atomic displacements of the interface of crystals with identical orientations. If such films are allowed to anneal many of the twin boundaries and microtwins disappear accompanied by grain growth.

5. Conclusions

1. The formation of continuous single crystal films of f.c.c. metals on alkali halides is a highly complex phenomenon. The orientation is not only determined by nucleation and growth of individual crystals but also by coalescence between crystals and depends in a complicated manner upon the experimental conditions.

2. Epitaxial nucleation is neither a necessary nor sufficient condition for the formation of single crystal films. It is not necessary because the orientation can develop during the growth of the individual crystals provided the state of minimum free energy can be reached. It is not sufficient because coalescence can change the predominant crystal orientation completely.

3. The influence of the experimental conditions on the initial phases of the condensation process can be understood both on the basis of the phenomenological and atomistic nucleation theories, however the former appears more realistic. The critical quantity is the Gibbs free energy $\Delta G_K(g^*)$ for the formation of a nucleus. This activation barrier does not exist in the atomistic theories, in which differences in the heat of adsorption ΔG_a or

in the activation energy for surface diffusion ΔG_D have to account for differences in experimental results (at constant rate N_i and temperature T).

4. Coalescence between crystals with different orientations is strongly influenced by the interfacial energy between the crystals and its anisotropy. For interfaces such as twin boundaries with low interfacial energy complicated coalescence orientations can be formed spontaneously.

5. The energy liberated during coalescence can initiate chemical reactions which may change the anisotropy of the surface free energy of the crystals and consequently their orientation and shape with minimum Gibbs free energy.

6. In the final stages of the film formation the tendency to form a plane parallel slab with minimum free surface energy σ lead to the formation of a film in which all crystals have a plane with low σ parallel to the substrate. The azimuthal alignment of the crystals can be better or worse than that of the crystals before coalescence.

7. The growth and structure of f.c.c. metal films on alkali halides is highly specific not only for each film substrate orientation, but also for the experimental conditions. In view of the many parameters and physical processes involved it is highly unlikely that a full understanding of the film growth can be obtained unless as many parameters as possible are eliminated (such as residual gases, surface condition), unless the experimental conditions are carefully controlled and unless artefacts (such as electron beam or annealing effects) are excluded.

This work was supported in part by the National Aeronautics and Space Administration under Contract No. R-05-030-001.

REFERENCES - PART II

(See Part I for Refs. [1 - 24])

[25] R. Lad, discussion remark to ref. [20], p. 500.

[26] H. Bethge and M. Krohn, in Adsorption et Croissance Cristalline, C.N.R.S., Paris 1965 (p. 389), and references cited there.

[27] A. Oberlin and M. Hucher, in Adsorption et Croissance Cristalline, C.N.R.S., Paris 1965 (p. 407).

[28] R. W. Adam and M. Harsdorff, Z. Naturforsch. 20a, 489 (1965).

[29] A. K. Green and E. Bauer, unpublished.

[30] R. F. Adamsky and R. E. LeBlanc, J. Vac. Sci. Techn. 2, 79 (1965).

[31] G. A. Bassett and D. W. Pashley, J. Inst. Metals 87, 449 (1958-9).

[32] J. W. Matthews and D. L. Allison, Phil. Mag. 8, 1283 (1963).

[33] J. L. Robins and T. N. Rhodin, Surface Sci. 2, 346 (1964).

[34] B. E. Sundquist and R. A. Oriani, J. Chem. Phys. 36, 2604 (1962).

[35] J. H. van der Merwe, Proc. Phys. Soc. A63, 616 (1950); J. Appl. Phys. 34, 117 (1963); in Single Crystal Films, ed. by M. H. Francombe and H. Sato, Pergamon Press, 1964 (p. 136).

[36] W. J. Dunning, in Adsorption et Croissance Cristalline, C.N.R.S., Paris 1965 (p. 369).

[37] H. Göttsche, Z. Naturforsch. 11a, 55 (1956).

[38] S. Ino, J. Phys. Soc. Japan 21, 346 (1966).

[39] E. Gillet and M. Gillet, C. R. Acad. Sci. 262, 359 (1966).

[40] E. Bauer, Z. Kristallogr. 110, 372 (1958).

[41] M. Ackerman, F. E. Stafford, and J. Drowart, J. Chem. Phys. 33, 1784 (1960).

[42] G. Zinsmeister, Intern. Symp. Basic Problems in Thin Film Physics, Clausthal-Göttingen, Sept. 1965.

[43] D. W. Pashley, M. J. Stowell, M. H. Jacobs, and T. J. Law, Phil. Mag. 10, 127 (1964).

[44] D. G. Fedak and N. A. Gjostein, Phys. Rev. Letters 16, 171 (1966).

[45] E. Bauer, unpublished.

[46] B. Honigmann, Gleichgewichts-und Wachstumsformen von Kristallen, Steinkopff, Darmstadt 1958, p. 110.

[47] I. L. Dillamore and R. E. Smallman, Phil. Mag. 12, 191 (1965).

[48] G. Menzer, Z. Kristallogr. 99, 410 (1938).

[49] A. Goswami, J. Sci. Industr. Res. 13B, 677 (1954).

[50] R. B. Kehoe, Phil. Mag. 2, 455 (1957).

FIGURE CAPTIONS

Fig. 1. Transmission diffraction pattern of (100) orientation (full circles) and of the four equivalent (110) orientations (open circles); see Part I.3.1.

Fig. 2. Dependence of the Gibbs free energy change ΔG, upon size g of condensed particle, (schematic). Discrete jumps at small g are approximated by smooth curves and oscillations are neglected. a) in an atomistic theory with nucleation barrier; b) in the phenomenological theory; c) in an atomostic theory without nucleation barrier; and d) dependence assumed in this work.

Fig. 3. Transmission diffraction pattern showing the a) (100), and b) (111) basic pattern (solid circles) and twin spots (open circles) observable by allowing rotations α about the origin of: $\alpha < 5°$ (large circles), $5° < \alpha < 12°$ (medium circles), and $12° < \alpha < 20°$ (small circles).

Table 1

Results of evaporations of f.c.c. metals onto crystals with NaCl structure from several authors

Ref.	Film	Substrate	Temperature (°C)	Deposition Rate (Å/min)	Cleaving environment	Number N of particles (in $10^{10}/cm^2$)	Average particle diam. $\bar{D}$ (Å)	Mean film thickness $\bar{t}$ (Å)
[14]	Au	NaCl	360	-	air	210		1
				-	(UHV)	120		
				-	air	35		25
				-	(UHV)	12		
[7]	Au	NaCl	20	-	air	110	130	12
					vac	74	100	4
[30]	Au,Ag	NaCl	300	50-200	vac	10-80	-	-
[31]	Au	NaCl	270	-	air	25 max	-	5
[32]	Ag	NaCl	300	-	air	22 max	-	-
[24]	Ag	NaCl	220-280	.5-3	UHV	.5-9	-	-
[33]	Au	MgO	210-280	-	UHV	35 max	-	-

Table 2

Crystallographic relations for multiple twinning

	Nomenclature	Plane parallel to substrate	Corresponding axes in plane parallel to substrate	Twin axis
Base orientation		(100)	$[0\bar{1}1]$	
1st twin	(100)-T1	$(\bar{1}\bar{2}2)$	$[4\bar{1}1]$	$[1\bar{1}1]$
Upper 2nd twin	(100)-$T2_u$	$(\bar{7}\bar{4}4)$	$[\bar{8}7\bar{7}]$	$[11\bar{1}]$
Lower 2nd twin	(100)-$T2_\ell$	$(14\bar{8})$	$[\bar{4},11,5]$	[111]
Base orientation		(111)	$[0\bar{1}1]$	
1st twin	(111)-T1	$(\bar{1}5\bar{1})$	$[4\bar{1}1]$	$[1\bar{1}1]$
Upper 2nd twin	(111)-$T2_u$	$(\bar{7},5,13)$	$[\bar{8}7\bar{7}]$	$[11\bar{1}]$
Lower 2nd twin	(111)-$T2_\ell$	$(\bar{1}\bar{1},1,\bar{1}\bar{1})$	$[\bar{4},11,5]$	[111]

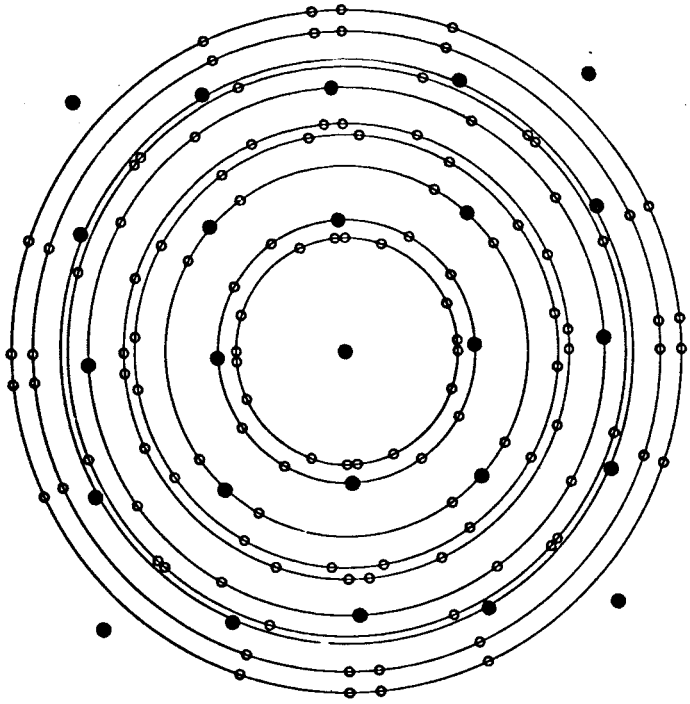

Fig. 1

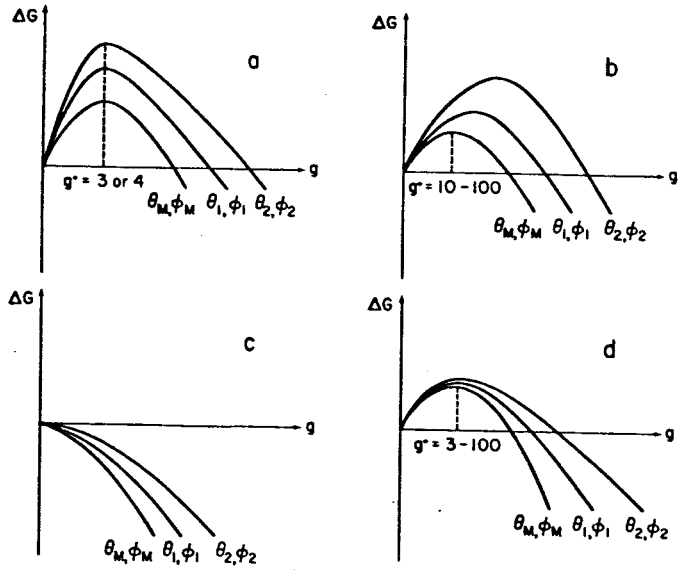
ΔG
a
g
g* = 3 or 4
θM,φM θ1,φ1 θ2,φ2
ΔG
b
g
g* = 10 - 100
θM,φM θ1,φ1 θ2,φ2
ΔG
c
g
θM,φM θ1,φ1 θ2,φ2
ΔG
d
g
g* = 3 - 100
θM,φM θ1,φ1 θ2,φ2

Fig. 2

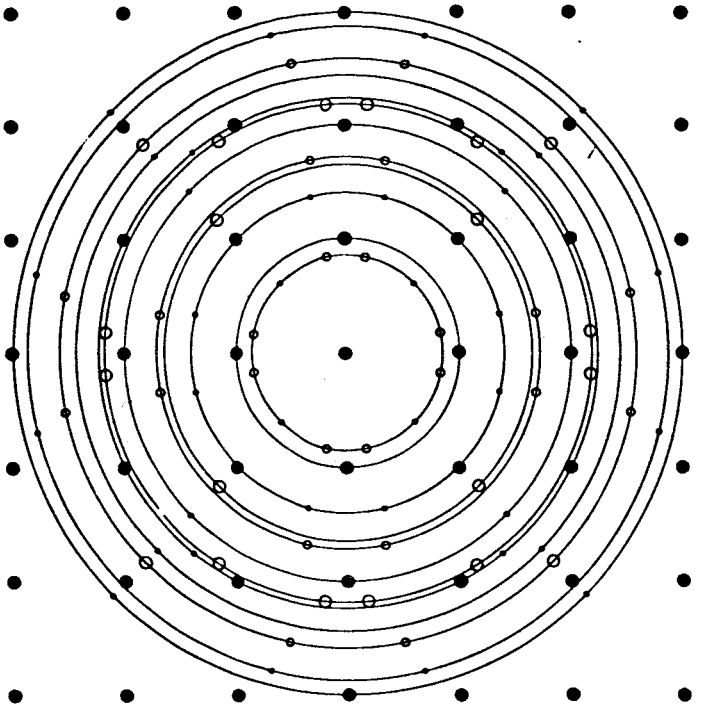

Fig. 3a

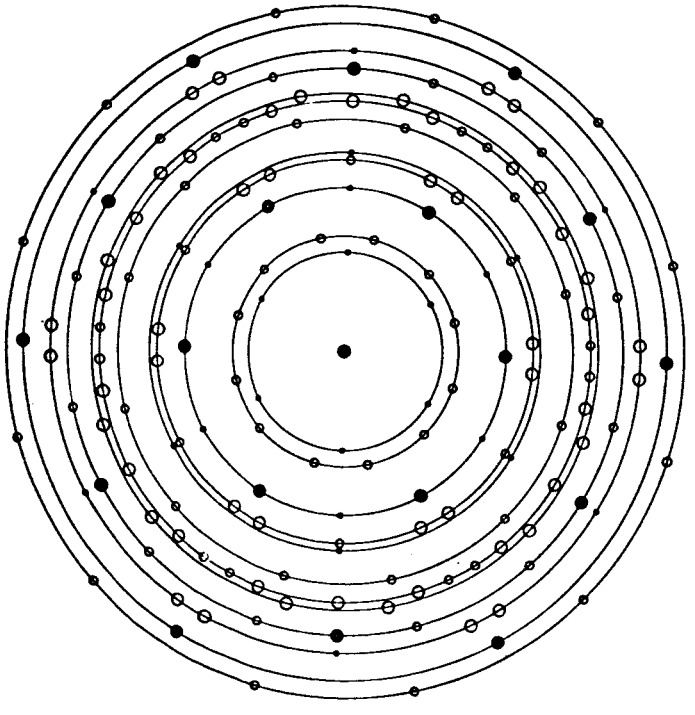

Fig. 3b

An Ultrahigh Vacuum Electron Microscope and Its Application to Work Function Studies

G. H. Turner and E. Bauer
Michelson Laboratory, China Lake, California 93555

In recent years there has been a marked increase of interest in surface phenomena many of which are well known to be very sensitive to residual gases. For example, an oxygen partial pressure of 5.10^{-9} torr has considerable influence on the electron emission from tungsten covered with adsorbed Ba. If one wants to obtain a basic understanding of the dependence of such surface phenomena on the submicroscopic structure of surfaces, a surface electron microscope is needed which works in the 10^{-10} torr region and in which the surfaces can be made atomically clean. With these goals in mind an U.H.V. surface electron microscope has been developed. The instrument operates currently in the emission and mirror microscopy modes. Low energy reflection microscopy and low energy electron diffraction modes are being incorporated. In addition, two quantitative integrating modes are possible at present: (1) measurement of total emission current, and (2) contact potential measurements.

The arrangement of the major components can be seen schematically in SLIDE 1. The electron optics consist of an electrostatic objective lens, electrostatic filter and magnetic intermediate and projector lenses. The specimen forms one element of the objective lens and can be heated or irradiated with light or electrons for emission microscopy. In the reflection and mirror modes of operation an electron beam originating at the electron gun is reflected at the specimen and subsequently imaged on the

Encl. (2)

fluorescent screen immediately below the viewing ports. The filter is essential in removing the inelastically scattered electrons in the reflection and diffraction mode. The intermediate and projector lenses have been given an additional degree of axial freedom in order to operate near the focal length minimum and to compensate for the large variation in optical properties of the objective lens when operated in the reflection mode.

The next SLIDE 2 is a view of the instrument itself. The all stainless steel construction allows baking up to 450°C. The base pressure is 2×10^{-10} torr. The specimen can be heated to 2800°K and can also be cleaned by ion bombardment. The design of the center electrode of the objective lens permits evaporation onto the specimen while in observation position. Residual gases, decomposition and desorption products can be analyzed by means of a mass spectrometer.

As an example of the application of the instrument, I would like to report some preliminary results on electron emission phenomena which are well known to be extremely sensitive to residual gases. This is especially true of the work function minimum observed in many alkali and alkaline earth films and in films of their oxides on refractory metals. The purpose of this study is to correlate the electron emission properties of surfaces (especially at the work function minimum) with the surface structure by combining the U.H.V. surface electron microscope with Low Energy Electron Diffraction. The experimental techniques and results are illustrated here for the system SrO on a (110) oriented W single crystal.

SrO was evaporated at several temperatures between 1500°K and 1700°K onto a W single crystal at various temperatures. Pressure during the

evaporations was from 2 - 7 x 10^{-10} torr. W surfaces had orientations near the ⟨110⟩ and were cleaned by electron bombardment above 2000°K before deposition. Light from a PEK 110 Hg arc lamp was focussed onto the specimen by quarts optics and photoelectric emission micrographs and photoelectric work function measurements were taken at intervals during deposition. Change in contact potential was also measured by the electron beam method. Similar depositions were made in a Varian Low Energy Electron Diffraction instrument to obtain information on the atomic arrangement of the surface. SLIDE 3 illustrates typical results for total photocurrent, curve (1), and photoelectric work function and contact potential change, curve (2), as a function of deposition time for W specimens at room temperature. There is no minimum observed in the work function as a function of film thickness. Low Energy Electron Diffraction shows that in this thickness range there is no ordered surface structure formed at the evaporation rates considered. Only an increase in background and a decrease in the intensity of the clean W diffraction spots is noted. The surface electron microscope shows uniform emission over the entire surface. Upon heating such a film, however, the surface structure passes through several distinct stages, until above 1950°K clean W is again observed. All of these stages are quite sensitive to film thickness and annealing time and temperature. Only the temperature range from 300°K to 1100°K will be considered in detail here.

SLIDE 4, curve (1), illustrates the change in apparent photoelectric work function as a function of increasing annealing temperature for SrO deposited on (110) oriented W at 300°K. Below about 650°K the work function

remains essentially constant and the photoelectric emission is uniform over the surface. As the annealing temperature rises above 650°K the photoelectric work function decreases and passes through a minimum at 820-870°K. Curve 2 is representative of the change in work function observed when SrO is deposited at higher specimen temperatures. Each point is taken from a separate evaporation and a somewhat sharper minimum is observed.

The next SLIDE 5 is typical of the lateral intensity distribution of photoemission occurring in this region of minimum work function. The magnification is $\sim$400 X. The high intensity emission centers can be correlated with the decrease in photoelectric work function and appear at reproducible sites on the W specimen which appear to be steps. Low Energy Electron Diffraction indicates that in the stepped regions of the crystal the (111) orientation of SrO as shown in SLIDE 6 is predominant. On the flat areas however, (100) oriented SrO and (110) oriented γ-Sr is mainly observed. In spite of the decrease in work function there is only a slight increase in total photoelectric emission. Increasing the annealing temperature above 1050°K results in the disappearance of the high emission centers and the ordered SrO and Sr structures. The work function rises several tenths of an electron volt and new diffraction patterns appear. It is one of these that appears in the proceedings and is not related to the work function minimum. This structure--like the others--is very sensitive to annealing time and temperature and can be interpreted as a strained Sr layer on a chemisorbed oxygen layer together with a structure similar to 100 oriented SrO in periodicity but with an intensity-voltage curve which is incompatible with those of (100) oriented SrO. At higher temperatures

the work function rises very rapidly and other structures appear that can be associated with the Sr-W-O and W-O system, and chemisorbed oxygen. Due to the complexity of the processes involved it is difficult at this stage of investigation to draw any quantitative conclusions.

Our results show, however, that the work function minimum occurs over a wide thickness range which is difficult to explain in terms of the widely accepted dipole layer theory. Adsorbed Sr freed as a result of SrO reacting with the W surface can also be excluded as a cause for the minimum for 2 reasons: (1) the minimum occurs at a temperature below which SrO reacts with W, and (2) free Sr is already present in the as-deposited film.

The preferred formation of 111 oriented SrO crystals in the regions where the high emission centers occur suggest that the work function minimum is associated with the (111) oriented SrO crystallites.

For a full understanding of the high emission of these centers more work is needed in which the use of the low energy electron reflection microscopy and low energy electron diffraction modes should be extremely helpful.

FIGURES

For Figs. 2, 3, and 5 see First Quarterly Progress Report, Encl. (3), Figs, 1, 2, and 3 respectively.

Fig. 1. Schematic of UHV electron microscope.

Fig. 4. Change of apparent work function with annealing and deposition temperature.

Fig. 6. LEED pattern of (111) oriented SrO.

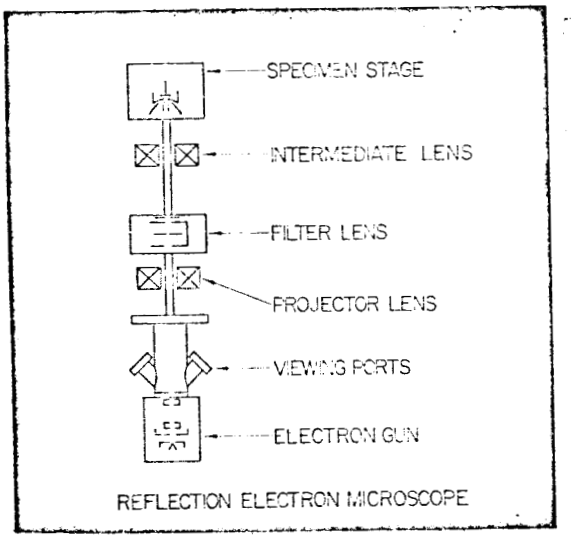

Fig. 1

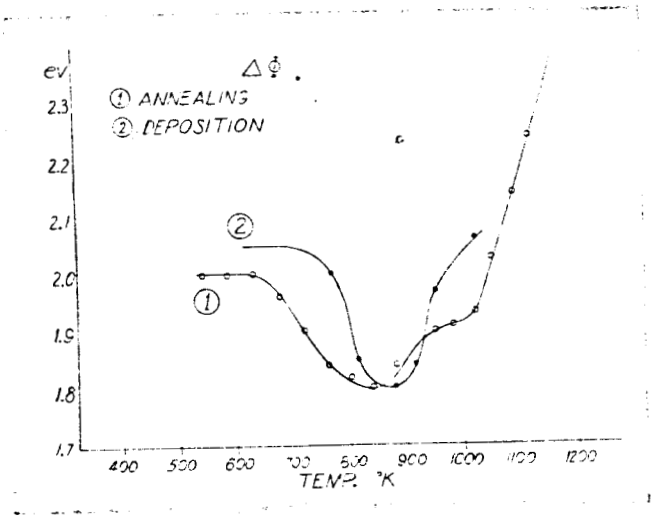

Fig. 4

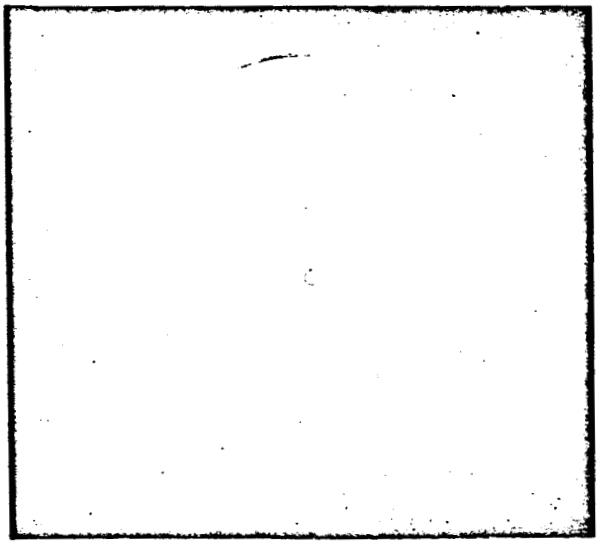

Fig. 6

Importance of Relativistic Effects in the Scattering of Slow Electrons, II

by atoms

H. N. Browne and E. Bauer
Michelson Laboratory, China Lake, California 93555

(Received 1 July 1966)

Our recent claim[1] (referred to here as I) that relativistic effects are of importance for the total and differential scattering cross sections of atoms for slow electrons has caused considerable controversy.[2,3] We attribute this to (1) lack of clarity of our letter due to its brevity, and (2) the difficulty of imagining a relativistic effect to be important in neutral atoms at low energies. The purpose of this letter is to clarify some of the misunderstandings and to present additional material strengthening our claim. The following critique has been made:

(1) It is inconsistent to use a nonrelativistic potential in the relativistic wave equation for the free electron and vice versa.[2]

(2) If different potentials are used in the relativistic and nonrelativistic equations such that they yield the correct levels for loosely bound states of the atoms, then the relativistic effects claimed in I disappear.[2]

(3) If the atom has a $\ell = 0$ ionic bound state with very small binding energy $E_B = \gamma^2$ (in Hartree atomic units) then the phase shift η for $\ell = 0$ and $k \to 0$ is given by $k \cot \eta \approx -\gamma$ irrespective of the short range part of the potential. The same is true for $\ell \neq 0$.[3] Therefore the $\Delta\eta_\ell = \eta_\ell^R - \eta_\ell^{NR} \to 0$ for $k \to 0$ if identical potentials are used in the nonrelativistic and relativistic Eqs. I(1) and I(2).

(4) The very low energy scattering phases are bad because long range effects are neglected in I.[3]

---

*This work was supported in part by the National Aeronautics and Space Administration under Grant No. R-05-030-001.

Encl (3)

(5) Figure 2 in I, which indicates a strong p-wave contribution, is in contradiction to the statement that relativistic effects are significant up to η_1 in Hg at 2 eV.[4]

Our replies to these critical remarks are as follows:

(1) It is obvious that a nonrelativistic potential V_{NR} should be used in the nonrelativistic wave Eq. I(1) and a relativistic potential V_R in the relativistic Eq. I(2) and that the results should be compared with each other, instead of comparing the results obtained by putting the same potential into both equations. However, relativistic potentials and nonrelativistic potentials obtained in the same approximation, e.g. in the Hartree approximation, differ very little from each other in the r-region in which the α^2 term in Eq. I(2) is significant, but differ considerably for larger r. If different results are obtained for the two cases using the corresponding wave equations it would only be natural to ascribe them to the differences in V(r) for larger r for two reasons: (1) it is well known that the scattering of slow electrons is strongly influenced by the outer parts of the atom, and (2) it is generally assumed that slow electrons do not penetrate very deeply into the atom. If a relativistic effect is to be demonstrated one has to make sure that the effective potentials differ only due to the relativistic terms. This was done in I. However, it may be argued that the differences in scattering cross sections caused by the differences in the effective potentials at very small r values may be partially or completely compensated by the potential differences for larger r if a self-consistent approach is used. This omission is corrected in Table I which gives the total elastic scattering cross sections for Hg using a self-consistent

approach, i.e. a nonrelativistic Hartree potential[5] in Eq. I(1) and relativistic Hartree potentials[6,7] in Eq. I(2). A comparison of the results, especially for 2 and 4 eV, shows that the differences in scattering cross sections caused by the differences in the effective potential at very small r values is not compensated by the potential differences at larger r values.

(2) In Rotenberg's method[2] the potentials are chosen in such a manner that the influence of the α^2-term in the relativistic Eq. I(2) on the energies of loosely bound states is compensated by differences in the potentials for larger r values to give identical energies for both cases (R and NR). It is therefore not surprising that the R and NR low energy scattering phases differ little. This was also noted by Mittleman.[8] A self-consistent nonrelativistic calculation however cannot give the same energies as a self-consistent relativistic calculation in the same approximation, as amply demonstrated in the literature, because it neglects certain physical effects such as the relativistic s-shift or the spin orbit coupling. Rotenberg's results, based on identical bound state energies in the R and NR cases, while correct, are irrelevant to our claim. ∧ therefore

(3) This argument is correct and our calculations are not in contradiction to it. Applied to the atom + electron case it says essentially that the probability of finding an electron with nearly zero energy near the nucleus is very small, whether the electron is bound or free. If this interpretation is accepted then the condition of the existence of a bound state appears unnecessary, i.e. $\Delta\eta_\ell = \eta_\ell^R - \eta_\ell^{NR} \to 0$ for $k \to 0$ even if no ionic bound ℓ states exist. This is already indicated in Fig. 3 of I in which the $\Delta\eta_\ell$ begin to decrease below about 10 eV and confirmed by the results of

Table II which gives the continuation of the data in Fig. 3 of I to lower energies. A similar behavior is observed for Hg. The total elastic scattering cross sections Q_R and Q_{NR} as obtained from the R and NR Eqs. I(1) and I(2) respectively, using Cohen's relativistic Hartree potential, are shown in Table III. These results indicate that Spruch's argument, while principally valid even without the existence of weakly bound ionic states, is applicable only to extremely low energies, and not to the low energy range considered in I. However, for the sake of clarity, the statement made in I that the relativistic effects decrease with increasing energy, due to the a^2 term should be made more precise by limiting the validity of the statement to the energy range used in electron beam experiments, i.e. from several tenth's of an eV ~~up to~~ several eV. This is the range with which our work is concerned, and was not mentioned in I. In the thermal energy range the effects decrease with energy. or on upwards

(4) This is true as follows from statements at the beginning and at the end of I: At the beginning it is pointed out that exchange and polarization are neglected, at the end it is pointed out that exchange and polarization have to be included in order to obtain reliable scattering cross sections for slow electrons. On the basis of our experience to date with scattering cross section calculations for heavy atoms, in which exchange and polarization are taken into account by an improved version of a method reported earlier,[9] we have little hope that reliable results for slow electrons can be obtained with the presently available atomic wave functions. Therefore exchange and polarization are neglected in I and here, so that the results, at least in the range below 10 eV, cannot be compared with experiment. But this has little influence on the subject of this paper. see below

- if judged by the degree of agreement with experiment -

(5) The strong difference in the p-wave contribution in Fig. 2 of I appears only for the Thomas-Fermi-Dirac potential, and for none of the other potentials investigated. The statement in I that relativistic effects are significant up to η_1 in Hg at 2 eV is therefore inaccurate. It is true only in general for the potentials studied.

We would like to add ~~a few additional~~ arguments to strengthen our claim made in I. Fradkin et al., and Rawitcher, have brought to our attention that relativistic effects have been shown to be of importance in the low energy scattering of electrons by a Coulomb potential.[10,11] An atomic potential, in the region where the α^2 term in Eq. I(2) is significant, is not very different from the Coulomb potential. This can be seen if the effective nuclear charge $Z(r)$ is expanded in a power series in r: $Z(r) = Z_o - ar + br^2 + \ldots$. If only the term linear in r is kept, we have $V(r) = \frac{Z_o}{r} - a$. For Hg, a = 640, 610 and 540 for the Mayers, Cohen and Hartree potentials, respectively. If $r = 10^{-3}$ the atomic potential deviates from the Coulomb potential by less than 1%; $V'(r) = -\frac{Z_o}{r^2} + b + \ldots$ and $V''(r) = 2\frac{Z_o}{r^3} + \ldots$ deviate even less. If a slow electron can penetrate into this region of an atom it will therefore see a similar potential as in the Coulomb case and similar effects are to be expected. The numerical calculations show that this is the case.[9] A comparison with positron scattering is of interest in this connection. As the relativistic effects are due to the region near the nucleus, no such effects would be expected in the positron case because of the repulsive nature of the potential near the nucleus. Corresponding differences between electron and positron scattering have been noted in the Coulomb case.[10,11] Our calculations for Hg show quite clearly the absence

of relativistic effects as caused by the α^2 term (column 1 versus 2 in Table IV), but indicate a relativistic effect due to the potential differences at larger r values (column 1 versus 3 in Table IV).

If the theoretical arguments for the importance of relativistic effects for the scattering of slow electrons by atoms should not be convincing enough, we would like to refer to the recent measurements of the Mott polarization of slow electrons scattered by Hg atoms.[12] The theoretical work of Schonfelder[13] should also be mentioned in this connection.

In conclusion, relativistic effects are important in the scattering of slow electrons by heavy atoms. They are in part due to the α^2 term in the relativistic wave equation, as shown in I, and in part due to the difference between relativistic and nonrelativistic potentials for larger r values, as shown here, especially for the positron case.

We would like to thank M. A. Coulthard, H. Deichsel, D. M. Fradkin, M. H. Mittleman, G. H. Rawitscher, M. Rotenberg, and L. Spruch for preprints, references, and correspondence.

Table I. Total elastic scattering cross sections of Hg for slow electrons using Hartree potentials in the nonrelativistic (NR) and relativistic (R) wave equations (in atomic units).

Energy (eV)	Hartree[5] NR	Mayers[6] R	Cohen[7] R
2	297	84.1	89.2
3	80.9	64.8	111
3.5	63.2	90.8	143
4	52.3	151	151
7	22.2	50.9	38.6
20	17.0	15.1	14.3
23	20.6	16.9	16.4
45	38.3	31.9	32.6
200	29.0	27.2	27.7
300	20.8	20.8	21.2

Table II. Scattering phases (mod π) for very slow electron scattering by Kr using the same potential in the relativistic (R) and nonrelativistic (NR) equations.

Energy	ℓ	R $\eta_\ell(j = \ell - \frac{1}{2})$	R $\eta_\ell(j = \ell + \frac{1}{2})$	NR η_ℓ
1	0		-.740717	-.815164
	1	.150244	.131645	.127995
	2	.000696	.000688	.000763
.5	0		-.532697	-.589755
	1	.048131	.042978	.041939
	2	.000131	.000129	.000141
.1	0		-.241708	-.269094
	1	.003968	.003594	.003514
.05	0		-.171445	-.190780
	1	.001370	.001242	.001232
.01	0		-.076826	-.085501
	1	.000121	.000110	.000109
.005	0		-.054288	-.060475
	1	.000043	.000039	.000039
.001	0		-.024265	-.027051
	1	.000004	.000004	.000003

Table III. Total elastic scattering cross sections of Hg for very slow electrons using Cohen's potential in R and NR equations (in atomic units).

Energy (eV)	1	.5	.1	.05	.01	.005	.001	.0001
R	175	314	669	773	877	885	891	893
NR	58.3	132	455	605	810	845	875	882

Table IV. Total elastic scattering cross sections of Hg for slow positrons using R and NR Hartree potentials in R and NR equations (in atomic units).

Energy (eV)	Cohen[7] R	Cohen[7] NR	Hartree[5] NR
2	48.8	48.5	61.8
20	33.6	33.5	40.1
200	16.6	16.6	17.7

REFERENCES

1. H. N. Browne and E. Bauer, Phys. Rev. Letters 16, 495 (1966).
2. M. Rotenberg, Phys. Rev. Letters 16, 969 (1966).
3. L. Spruch, ~~to be published~~ Phys. Rev. Letters 16, 1137 (1966)
4. L. Spruch, private communication.
5. D. R. Hartree and W. Hartree, Proc. Roy. Soc. A149, 210 (1935).
6. D. F. Mayers, Proc. Roy. Soc. A241, 93 (1957).
7. S. Cohen, Rand Corp. Rep. RM-2272-AEC (1958).
8. M. H. Mittleman, private communication.
9. E. Bauer and H. N. Browne, in Atomic Collision Processes, edited by M. R. C. McDowell (North-Holland Publishing Company, Amsterdam, 1964), p. 16.
10. D. M. Fradkin, T. A. Weber, and C. L. Hammer, Ann. Physics 27, 338 (1964).
11. G. H. Rawitscher, Phys. Letters 9, 337 (1964).
12. H. Deichsel, E. Reichert, and H. Steidl, Z. Physik 189, 212 (1966).
13. J. L. Schonfelder, Proc. Phys. Soc. 87, 163 (1966).

x 10